VIP Electrocatalysis

DOI: 10.1002/anie.200703331

Efficient Oxygen Reduction Fuel Cell Electrocatalysis on Voltammetrically Dealloyed Pt–Cu–Co Nanoparticles**

*Ratndeep Srivastava, Prasanna Mani, Nathan Hahn, and Peter Strasser**

The electrocatalytic oxygen reduction reaction (ORR) on noble metal surfaces [Eq. (1), RHE = reversible hydrogen electrode] is one of the most widely studied reactions in electrochemistry. Its fundamental scientific and technological importance is based on the fact that the oxygen/water half-cell reaction is a strongly oxidizing and ubiquitous redox couple. Combined with an electron-supplying redox process, such as shown in Equation (2), a direct electrochemical conversion of

$$O_2 + 4H^+ + 4e^- \rightarrow 2H_2O \quad E_0 = +1.23\ \text{V vs. RHE} \tag{1}$$

$$H_2 \rightarrow 2H^+ + 2e^- \quad E_0 = 0\ \text{V vs. RHE}, \tag{2}$$

the overall Gibbs energy of reaction into electrical potentials is achieved. This conversion is the scientific basis for electrochemical conversion in fuel cells[1] or metal–air batteries.[2,3] The ORR is also used in oxygen depolarization cathodes (ODC) in modern chlorine technologies,[4,5] in which it replaces the hydrogen evolution process to improve electrical efficiencies. The reverse ORR process, that is, the evolution of oxygen from water, is crucial for efficient water (photo)-electrolysis[6,7] into hydrogen or in metal electrodeposition processes in the semiconductor industry.[2]

In polymer electrolyte membrane fuel cells (PEMFCs), the ORR electrode catalyst material of choice has been platinum for decades. The ORR on Pt, however, is irreversible, thus causing overpotentials and losses in fuel-cell efficiency. Much research has been dedicated to the identification of more efficient catalysts, that is, materials with reduced precious-metal content and improved ORR activity.[8] Pt-rich alloys, most prominently Pt–Co formulations, have shown promise, with state-of-art activity improvements of two to three times over pure Pt.[9,10] However, a material with an at least fourfold activity improvement, deemed crucial for automotive applications, has remained elusive to date.[11]

Herein, we report on carbon-supported Pt–Cu–Co ternary alloy nanoparticle electrocatalysts with previously unachieved four- to fivefold ORR activity improvements. We demonstrate the catalytic activities on rotating disk electrodes (RDEs) as well as in real H_2/O_2 fuel-cell devices. The active catalyst phase is formed in situ from Pt-poor (ca. 20 atom % Pt) alloy precursors by voltammetric dealloying, that is, partial metal dissolution. In particular, we consider three alloy precursors: $Pt_{20}Cu_{60}Co_{20}$, $Pt_{20}Cu_{20}Co_{60}$, and $Pt_{20}Cu_{40}Co_{40}$. The dealloying procedure selectively dissolves base metal atoms near the particle surfaces [Eqs. (3) and (4), NHE = normal hydrogen electrode] and forms Pt-

$$Cu \rightarrow Cu^{2+} + 2e^- \quad E_0 = +0.34\ \text{V vs. NHE} \tag{3}$$

$$Co \rightarrow Co^{2+} + 2e^- \quad E_0 = -0.28\ \text{V vs. NHE} \tag{4}$$

enriched core–shell particle structures. Since metal dissolution into the membrane electrolyte has very detrimental effects in fuel cells, we also developed a new procedure to form the active catalyst phase in situ inside a fuel-cell electrode layer without compromising the membrane conductance.

Figure 1 schematically illustrates our novel three-step procedure for preparation of the active catalyst phase. In step 1, the alloy precursor is applied in the cathode of a fuel-cell membrane–electrode assembly (MEA). During step 2, a cyclic voltammetric treatment selectively dissolves the less-noble metal atoms (mostly Cu) from the alloy particle surface. The Cu atoms migrate into the nafion polyelectrolyte and get trapped at negatively charged sulfonic acid groups. In step 3, the MEA is chemically treated with an inorganic acid, which results in complete exchange of Cu ions inside the polyelectrolyte with protons. After step 3, the catalyst has been converted into its active phase and is ready for use.

To evaluate the intrinsic activities of the ternary Pt alloy catalyst precursors, we performed steps 1–3 using thin catalyst/nafion films attached to a glassy carbon RDE in liquid acid electrolytes. RDE studies allow accurate correction of ohmic and transport overpotentials and therefore yield reliable estimates of upper bounds of intrinsic catalytic activities.[10,12] Since a liquid acid electrolyte is used in RDE tests, steps 2 and 3 occur simultaneously during the voltammetric pretreatment of the precursor. Figure 2 shows the ORR activity during sweep voltammetry of the three ternary catalysts. The sigmoidal shape of the ORR current–voltage characteristic is shifted to more positive potentials, indicating ORR activity at much lower overpotentials. Comparison of their Pt-surface-area-based activities and their Pt-mass-based activities (inset) with pure Pt revealed an unprecedented four-

[*] R. Srivastava, Dr. P. Mani, N. Hahn, Prof. P. Strasser
Department of Chemical and Biomolecular Engineering
University of Houston
4800 Calhoun Road Eng Bldg 1 S226
Houston, TX (USA)
Fax: (+1) 713-743-4323
E-mail: pstrasser@uh.edu

[**] This work was supported by the Department of Energy (Lab04-20) and by a TcSUH seed grant. Acknowledgment is also made to the Donors of the American Chemical Society Petroleum Research Fund for partial support of this research (grant no. 44165).

Supporting information for this article is available on the WWW under http://www.angewandte.org or from the author.

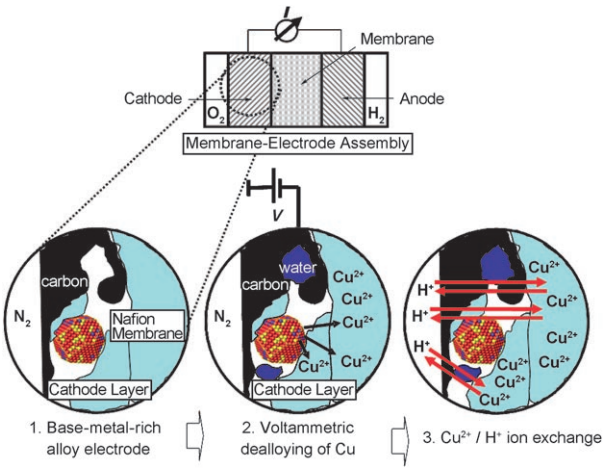

Figure 1. A novel three-step procedure for in situ voltammetric dealloying of base-metal-rich Pt–Cu–Co nanoparticle catalysts inside fuel-cell electrode layers. The top frame illustrates a membrane–electrode assembly of a H_2/O_2 fuel cell. In situ formation of the active catalyst phase involves the following steps: Step 1: Base-metal-rich Pt-alloy nanoparticles (red balls) are used as cathode catalysts for the oxygen reduction reaction. Step 2: The active phase of the catalysts is formed in the dealloying process. Step 3: Because leached Cu ions inside the fuel-cell membrane or electrode are detrimental, they are removed by chemical ion exchange.

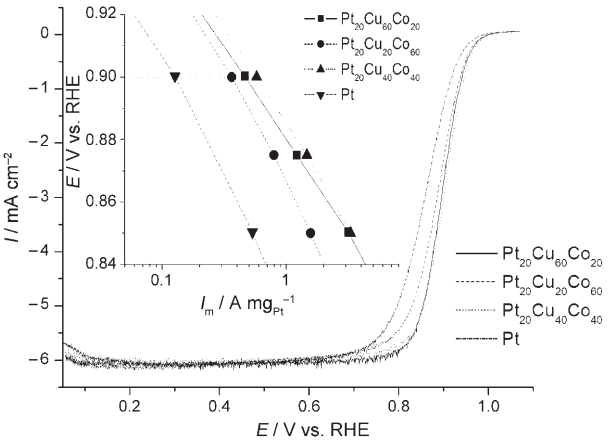

Figure 2. Oxygen reduction reaction (ORR) activity measurements of Pt–Cu–Co ternary alloy nanoparticle catalysts in an RDE setup. Inset: Pt-mass-based activities (A mg$_{Pt}^{-1}$) over a range of electrode potentials for which the surface catalysis is rate-determining (kinetically controlled region).

to fivefold improvement over a wide potential range. For instance, dealloyed $Pt_{20}Cu_{40}Co_{40}$ exhibited 0.6 A mg$_{Pt}^{-1}$ compared to 0.12 A mg$_{Pt}^{-1}$ for pure Pt.

For more detailed insight in the early stages of the Cu dealloying process inside a fuel-cell membrane–electrode assembly, we studied the system by cyclic voltammetry (CV, Figure 3). The initial trace (solid line) showed strong bulk Cu dissolution on the anodic scan between 0.3 and 0.5 V as well as some Cu redeposition (0.05–0.3 V) on the return scan. This result is consistent with the fact that much Cu had segregated to the Pt–Cu alloy surface of the annealed precusor particles.

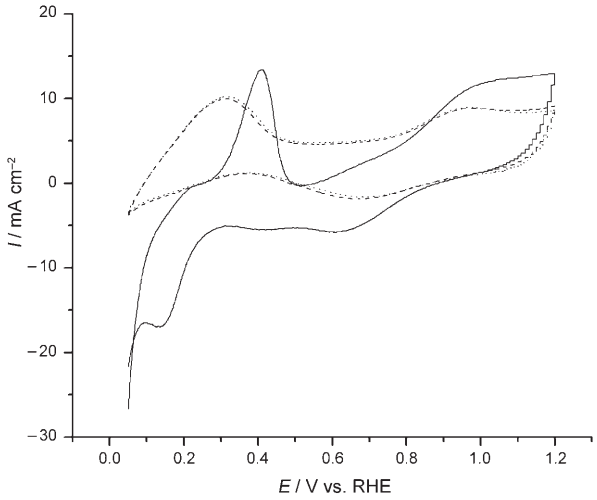

Figure 3. Selective electrochemical dissolution of Cu from $Pt_{20}Cu_{60}Co_{20}$ precursor catalysts during voltammetric pretreatment (voltammetric dealloying). Initial scan (——), trace after five potential cycles of Cu dealloying (-----), trace after 250 potential cycles (••••). The Pt-like voltammogram after dealloying indicates completion of Cu/Co dissolution. Conditions: $T_{cell} = 30\,°C$, anode H_2, cathode N_2.

After five scans, the response of the dealloyed catalyst started to resemble that of a Pt-rich catalyst surface with hydrogen adsorption and desorption emerging in the 0.05–0.4 V region and in the platinum oxide formation region above 0.7 V (dashed line). After dealloying over about 250 cycles (dotted line), the resulting voltammogram resembles that of pure Pt, thus supporting our hypothesis that the dealloying process results in a stable catalyst with an essentially pure Pt surface. Compositional studies of dealloyed Pt–Co have shown that Co atoms are more stable than Cu atoms against dissolution from Pt lattices,[9] resulting in a Pt- and Co-atom-enriched active catalyst surface.

Structural X-ray diffraction analysis was consistent with our voltammetric dealloying study. As Figure S1 in the Supporting Information shows, all three alloy-particle catalysts showed face-centered cubic (fcc) disordered alloy structures with the (111) reflection shifted to higher 2θ values compared to pure Pt. Residual unalloyed Cu ($Pt_{20}Cu_{60}Co_{20}$ and $Pt_{20}Cu_{40}Co_{40}$) and Co particles ($Pt_{20}Cu_{20}Co_{60}$) with large size showed sharp characteristic reflections.

Figures 4 and 5 and Table 1 demonstrate the cell performance and the catalytic ORR activity of the carbon-supported dealloyed catalysts (20–28 wt% Pt loading) in fuel-cell environments benchmarked against a carbon-supported 30 wt% and a 45 wt% Pt standard. The 45 wt% catalyst is commonly used as the Pt standard cathode electrocatalyst.[10] We also compared our ternary catalysts to a $Pt_{25}Co_{75}$ catalyst to show the synergies between Co and Cu. All three ternary alloy catalysts exhibited much higher cell potentials (Figure 4) over the entire range of current densities. The high-current region, in which gas and proton transport determines the overall current, gives evidence that the dealloying procedure had no detrimental effect on the transport characteristics of the fuel-cell electrodes or membrane.

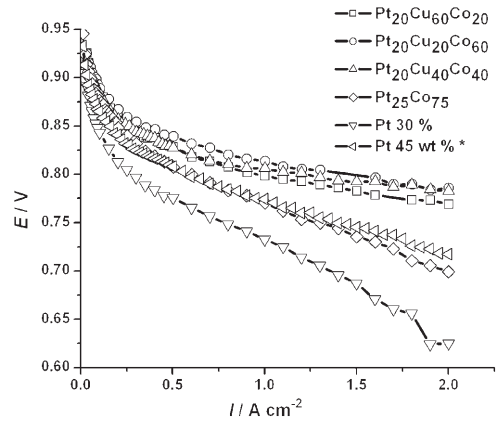

Figure 4. Polarization curves of 10-cm^2 single H_2/O_2 fuel cells using dealloyed ternary Pt–Cu–Co cathode catalysts. Conditions: $T_{cell}=80\,^{\circ}C$, $P_{total}=150$ kPa; see the Supporting Information for details. The standard Pt cathode electrocatalyst is indicated by *.

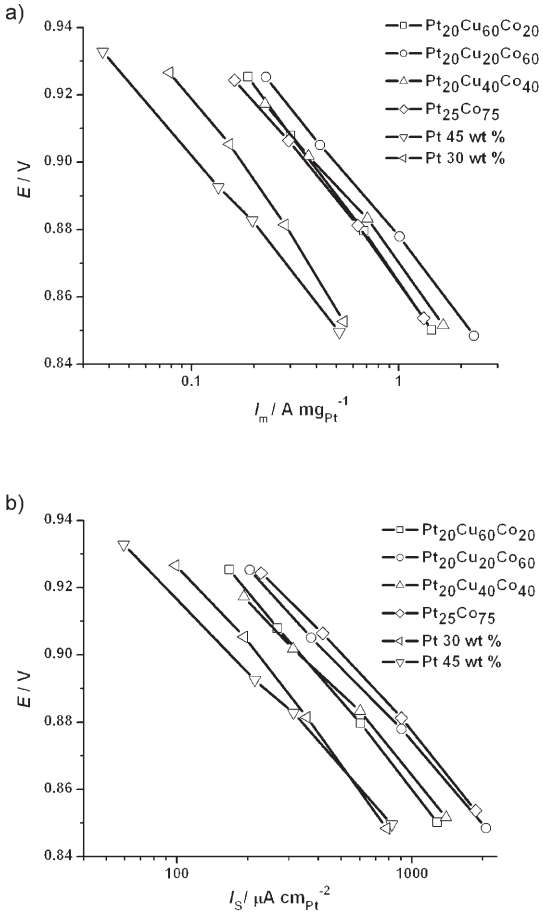

Figure 5. Oxygen reduction catalysis activities of dealloyed ternary alloys expressed in a) Pt-mass-based activity (A mg$_{Pt}^{-1}$) and b) Pt-surface-area-based (specific) activity (µA cm^{-2}). The cell potential is plotted over the corresponding intrinsic catalyst activities in the potential region in which the surface chemistry is rate-determining.

Detailed catalytic ORR activities on a Pt-surface-area and Pt-mass basis are reported in Figures 5 and S2a,b in the Supporting Information and in Table 1. All dealloyed base-metal-rich catalysts exhibit previously unachieved[10,13,14] four- to fivefold Pt-mass-based activity improvements over Pt. Figure 5 also reports the significant activity improvement of about 50% at 0.9 V caused by adding Cu to a $Pt_{25}Co_{75}$ catalyst.

Table 1: Alloy composition, electrode Pt loadings, surface areas, and ORR activities at 0.9 V for ternary Pt–Cu–Co alloy nanoparticle electrocatalysts.

Pt	Cu	Co	Cathode Pt loading	ECSA	Mass activity	Specific activity
	[atom%]		[mg$_{Pt}$ cm^{-2}]	[m^2 g^{-1}]	[A mg$_{Pt}^{-1}$]	[µA cm$_{Pt}^{-2}$]
20	60	20	0.183	112	0.37	337
20	40	40	0.150	117	0.39	340
20	20	60	0.150	111	0.49	441
25	0	75	0.146	70	0.34	491
100	0	0	0.149	79	0.16[a]	209
100	0	0	0.313	62	0.10[b]	165

[a] 30 wt% Pt. [b] 45 wt% Pt.

The electrochemical surface-area data of the alloy catalysts (Table 1 and Figure S2c in the Supporting Information) show that the dealloying process resulted in an almost twofold increase in active-particle surface area compared to the 45 wt% standard catalyst. This increase might be caused by surface roughening or particle break-up during dissolution. While contributing to the improved activity, the surface-area change fails to fully account for the observed four- to fivefold activity gains. We therefore suspect that more favorable structural characteristics, such as Pt–Pt surface interatomic distances of the dealloyed particles, play a key role in the enhancement mechanism.

To arrive at a structural hypothesis for the dealloyed catalysts, we invoke our structural and compositional analysis, which indicates that the dealloying procedure removed base metal atoms from the particle surface. The thickness of the dealloyed region is likely to dependend on the starting stoichiometry, alloy uniformity, and detailed dealloying conditions. We hypothesize that the active catalyst phase is represented by a core–shell particle as illustrated in Figure 6.

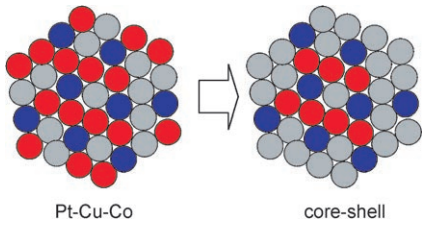

Figure 6. Formation of a Pt-enriched core–shell alloy nanoparticle by voltammetric dealloying of a Cu-rich alloy precursor (Pt gray, Cu red, Co blue).

A Pt-enriched shell (with some residual Co atoms) surrounds a base-metal-rich particle core. The distinct structural and electronic characteristics of the alloy core are likely to affect those of the surface Pt layers, thus modifying chemisorption energies and activation barriers of elementary steps of the ORR process.[15–17]

We also evaluated the electrochemical stability of the dealloyed catalysts by monitoring the changes in electrochemical surface area during voltage cycling (Figure S3 in the Supporting Information). Generally, the surface area of Pt-particle catalysts in electrochemical environments decreases significantly owing to Ostwald growth or dissolution.[18–23] Voltage cycling between 0.5 and 1 V resulted in a relative surface area loss of about 15% after 10000 cycles and 35% after 30000 cycles for the $Pt_{20}Cu_{20}Co_{60}$ and $Pt_{20}Cu_{40}Co_{40}$ alloy catalysts. This finding is very similar to the observed losses of pure Pt.[18,19,23] Cycling between 0.5 and 1.2 V resulted in a severe decrease in surface area by 60% after 10000 cycles, again in line with Pt stability measurements.[18]

In conclusion, we have reported a new class of voltammetrically formed Pt-poor ORR alloy particle electrocatalysts and presented a preparation method that lends itself well to PEMFC electrode layers. In fuel cells, the catalysts exhibited unprecedented ORR activities of up to 0.5 $A\,mg_{Pt}^{-1}$. Considering the technological PEMFC Pt mass activity target of 0.44 $A\,mg_{Pt}^{-1}$,[11] the presented catalyst class holds promise to help overcome today's performance challenges in automotive fuel-cell catalysis.

Experimental Section

Alloy precursors with Pt/Cu/Co stoichiometries of 20:60:20, 20:20:60, and 20:40:40 were prepared from commercial carbon-supported Pt nanoparticles (30% Pt by weight, TKK Inc.) mixed with Cu and Co salt solutions through an impregnation–freeze-drying–reductive-annealing method.[9]

RDE activity measurements were performed in a three-electrode configuration on a 5 mm glassy carbon disk electrode in 0.1M $HClO_4$ electrolyte.

Fuel-cell measurements were carried out using 10-cm^2 catalyzed cells, nafion membranes (NRE 212), 40 wt% Pt anode catalysts (0.4 $mg_{Pt}\,cm^{-2}$), and the ternary alloy precursor employed as cathodes. Voltammetric dealloying was performed at room temperature by cycling the cathode potential between 0.5 and 1 V vs. RHE under nitrogen flow. Ion exchange was performed using 1M sulfuric acid at 80°C for 2 h.

Detailed descriptions of all experimental procedures are given in the Supporting Information.

Received: July 24, 2007
Published online: September 24, 2007

Keywords: electrochemistry · energy conversion · intermetallic phases · nanostructures · voltammetry

[1] *Handbook of Fuel Cells—Fundamentals, Technology, and Applications* (Eds: W. Vielstich, A. Lamm, H. Gasteiger), Wiley, Chichester, UK, **2003**.
[2] J. O. Bockris, A. K. N. Reddy, *Modern Electrochemistry 2B: Electrodics in Chemistry, Engineering, Biology, and Environmental Science*, *Vol. 2B*, Kluwer Academic, New York, **2000**.
[3] J. O. M. Bockris, A. K. N. Reddy, M. Gamboa-Aldeco, *Modern Electrochemistry 2A: Fundamentals of Electrodics*, *Vol. 2A*, 2nd ed., Plenum, New York, **1998**.
[4] T. F. O'Brien, T. V. Bommaraju, F. Hine, *Handbook of Chlor Alkali Technology*, Springer, New York, **2005**.
[5] J. Moorhouse, *Modern Chlor-Alkali Technology*, Blackwell Publishing Limited, New York, **2001**.
[6] O. Khaselev, J. R. Turner, *Science* **1998**, *280*, 425–427.
[7] J. A. Turner, *Science* **1999**, *285*, 687–689.
[8] D. Thompsett in *Handbook of Fuel Cells—Fundamentals, Technology and Applications*, *Vol. 3* (Eds.: W. Vielstich, A. Lamm, H. A. Gasteiger), Wiley, New York, **2003**, chap. 437, p. 467.
[9] S. Koh, J. Leisch, M. F. Toney, P. Strasser, *J. Phys. Chem. C* **2007**, *111*, 3744–3752.
[10] H. A. Gasteiger, S. S. Kocha, B. Sompalli, F. T. Wagner, *Appl. Catal. B* **2005**, *56*, 9–35.
[11] Department of Energy—Multi-Year Research and Development Plan—3.4 Fuel Cells: Table 3.4.12 Electrocatalyst Targets for Transportation Applications, *Journal*, **2007** http://www.eere.energy.gov/hydrogenandfuelcells/mypp/, Vol. 3.4.-24.
[12] T. J. Schmidt, H. A. Gasteiger, G. D. Stab, P. M. Urban, D. M. Kolb, R. J. Behm, *J. Electrochem. Soc.* **1998**, *145*, 2354–2358.
[13] E. Antolini, *Appl. Catal. B* **2007**, *74*, 324–336.
[14] E. Antolini, *Appl. Catal. B* **2007**, *74*, 338–351.
[15] V. Stamenkovic, B. S. Moon, K. J. Mayerhofer, P. N. Ross, N. Markovic, J. Rossmeisl, J. Greeley, J. K. Norskov, *Angew. Chem.* **2006**, *118*, 2963–2967; *Angew. Chem. Int. Ed.* **2006**, *45*, 2897–2901.
[16] V. Stamenkovic, B. S. Mun, M. Arenz, K. J. J. Mayerhofer, C. A. Lucas, G. Wang, P. N. Ross, N. Markovic, *Nat. Mater.* **2007**, *6*, 241.
[17] V. R. Stamenkovic, B. Fowler, B. S. Mun, G. Wang, P. N. Ross, C. A. Lucas, N. M. Markovic, *Science* **2007**, *315*, 493.
[18] P. J. Ferreira, G. J. La O', Y. Shao-Horn, D. Morgan, R. Makharia, S. Kocha, H. Gasteiger, *J. Electrochem. Soc.* **2005**, *152*, A2256–A2271.
[19] B. Merzougui, S. Swathirajan, *J. Electrochem. Soc.* **2006**, *153*, A2220–A2226.
[20] E. Guilminot, A. Corcella, F. Charlot, F. Maillard, M. Chatenet, *J. Electrochem. Soc.* **2007**, *154*, B96–B105.
[21] J. Xie, D. L. Wood, K. L. More, P. Atanassov, R. L. Borup, *J. Electrochem. Soc.* **2005**, *152*, A1011–A1020.
[22] H. R. Colon-Mercado, B. N. Popov, *J. Power Sources* **2006**, *155*, 253–263.
[23] Y. Shao, G. Yin, Y. Gao, P. Shi, *J. Electrochem. Soc.* **2006**, *153*, A1093–A1097.

